It takes two to tango: Investigating the fuzzy interaction between tau and tubulin C-terminal tails

*Jules Marien[1,2], Chantal Prévost[1,2], and Sophie Sacquin-Mora[1,2]**

[1]CNRS, Université de Paris, UPR 9080, Laboratoire de Biochimie Théorique,

13 rue Pierre et Marie Curie, 75005 Paris, France

[2]Institut de Biologie Physico-Chimique-Fondation Edmond de Rotschild,

PSL Research University, Paris, France

*Corresponding author e-mail: sacquin@ibpc.fr

Running title : Disordered tubulin tails enhance tau binding on microtubules.

Keywords: Molecular Dynamics, protein interactions, tubulin, tau, disordered proteins

A preliminary version of this work was deposited in bioRxiv, doi: https://doi.org/

Abstract

The microtubule-associated protein (MAP) tau plays a key role in the regulation of microtubule assembly and spatial organisation. Tau hyperphosphorylation affects its binding on the tubulin surface and has been shown to be involved in several pathologies such as Alzheimer disease. As the tau binding site on the microtubule lays close to the disordered and highly flexible tubulin C-terminal tails (CTTs), these are likely to impact the tau-tubulin interaction. Since the disordered tubulin CTTs are missing from the available experimental structures, we used homology modeling to build two complete models of tubulin heterotrimers with different isotypes for the β-tubulin subunit (βI/αI/βI and βIII/αI/βIII). We then performed long timescale classical Molecular Dynamics simulations for the tauR2-tubulin assembly (in systems with and without CTTs) and analyzed the resulting trajectories to obtain a detailed view of the protein interface in the complex and the impact of the CTTs on the stability of this assembly. Additional analyses of the CTTs mobility in the presence, or in the absence, of tau also highlight how tau might modulate the CTTs activity as hooks that are involved in the recruitment of several MAPs.

1. Introduction

α and β-tubulins are the building blocks of microtubules (MTs), a central element of the cell cytoskeleton, which plays an essential part in cell division, signaling and intracellular transport.[1] The assembly of α/β-tubulin heterodimers leads to the formation of dynamic tubular fibers. Each tubulin protein is formed of a well-defined globular domain (core), ending with a disordered and negatively charged C-terminal tail (CTT). All cells contain multiple variants (known as isotypes) of α and β-tubulin. While the sequence of the tubulin body is highly conserved, most of the sequence variation between isotypes is located on the CTTs, and it appears that these isotypes are not functionally interchangeable,[2, 3] as they might modulate the MT assembly,[4] dynamics[5] and interactions with other proteins.[6] In addition, tubulin CTTs are targets for many post-translational modifications (PTMs), and the diversity induced by these genetic and chemical variations is often referred to as the *tubulin code*, and acts as a fine regulator of microtubule function.[7, 8] In particular, the tubulin tails display different mobility patterns,[9] which can contribute to the modulation of MT dynamics[10] and interactions with motor proteins such as kinesin and dynein[11] and several intrinsically disordered proteins, including tau.[12-15]

Tau is a long (441 amino acids) disordered Microtubule Associated Protein (MAP), which is abundant in brain an neuronal tissues (where it constitutes more than 80% of MAPs).[16] It regulates the MTs assembly and spatial organization,[17] and controls the motility of motor proteins on MTs.[18-21] Tau is involved in numerous neurodegenerative diseases, named tauopathies, including Alzheimer's disease (AD), which are characterized by fibrillar aggregation.[22] The binding of tau on MTs, and its propensity to

aggregate are affected by PTMs, in particular the hyperphosphorylation of tau has been shown to be involved in several pathologies.[23] For example, in AD brains, tau is found to be phosphorylated on more than 20 positions, mostly serine and threonine residues, and these PTMs impair the protein interaction and its stabilization of microtubules.[24, 25] Due to the disordered nature of tau, the tau/MT assembly is a *fuzzy complex*,[26, 27] which remains difficult to characterize with classical structural biology approaches. In particular, the disordered CTTs do not appear in the tubulin structures obtained by crystallography or cryo-EM that are currently deposited in the Protein Data Bank[28] (PDB).

In this perspective, we combined homology modeling and molecular dynamics (MD) simulations to build a complete model, including the CTTs, of the complex formed by the β/α/β tubulin heterotrimer and the tau R2 domain for two tubulin isotypes (βI/αI/βI and βIII/αI/βIII). We used the resulting trajectories to investigate the impact of the tubulin CTTs on the tau/tubulin interaction, and monitor the contacts formed by the partners along time to identify residues that play a key part in the protein interface. In particular, specific attention was payed to tau serine residues, as they are likely to be phosphorylated in tauopathies. We also investigated the CTTs mobility in the presence, or in the absence, of tau-R2 on the tubulin surface.

2. Material and Methods

Building the tubulin C-terminal tails and selecting starting models for the simulations

We used the structure of the complex formed by two β- and one α-tubulin subunits bound with the R2 domain of tau (a 30-residues fragment ranging from Lys274 to

Table 1: Sequences of the tubulin C-terminal tails.

Isotype	Sequence	Length
αI (D0vWZ0)	SVEGEGEEEGEEY	13
βI (W5PPT6)	DATAEEEE--DFGEEAEEEA	18
βIII (Q13509)	DATAEEEG--EMYEDDEEESEAQGPK	24

Gly304) obtained by cryo-EM (pdb: 6CVN)[29] as a template. As this structure does not account for the tubulin CTTs, we used Modeller v10.2[30, 31] to build two different isotypes, βI/αI/βI and βIII/αI/βIII, using sequences from sheep tubulin (which were chosen to fit experiments from experimental collaborators) for the αI (gene TUBAIA, Uniprot[32] accession number D0VWZ0) and βI (gene TUBB, Uniprot accession number W5PPT6) subunits, and from human tubulin (since the sheep sequence is not available) for the βIII subunit (gene TUBB3, Uniprot accession number Q13509), see Table 1. The Modeller process is based on a classic comparative modeling method consisting of four sequential steps: template selection, template-target alignment, model building and a final model evaluation. Because of the high similarity between the target sequences and the structural templates (over 75% sequence identity), there was no need for a manual rearrangement of the alignments.

To select non-redundant CTT structures as starting points for the simulations, we used the gmx_cluster tool from the GROMACS[33] suite, with clustering cutoffs on the CTT backbones of 8.5 Å and 9.5 Å, for the βI/αI/βI and βIII/αI/βIII systems respectively. For both systems, we selected a representative structure from the two most populated clusters. In addition, an outlier structure (identified by increasing the cutoffs to 10 Å and 11 Å respectively) was also selected for both systems. These sets of three

structures for each isotype were used as seeds for the MD simulations to efficiently sample the CTTs conformational space and are shown in Figure 1.

All-atom Molecular Dynamics simulations

Simulation setup All systems (see Table 2) were prepared using the solution builder module from the CHARMM-GUI[34] (https://www.charmm-gui.org/) input generator. The complete system was solvated with TIP3P water molecules[35] in rectangular boxes (with a larger box for the βIII/αI/βIII isotype accounting for the longer CTT of βIII), in a physiological solution of NaCl (0.15 mol.L^{-1}). We used NAMD v2.14,[36] with the CHARMM36m[37] force-field under periodic boundary conditions with the Particle Mesh Ewald (PME) method,[38] and covalent bonds involving hydrogen atomes were constrained using the SHAKE algorithm.[39] We used a time step of 2 fs, and data acquisition was set every 100 ps. The simulation procedure starts with 10000 steps of energy minimization and 2 ns of equilibration in the NVT ensemble, which are followed by 200 ns of production in the NPT ensemble at 300K. The temperature was simulated through Langevin dynamics, and pressure was set at 1 atm using a Nose-Hoover Langevin Piston algorithm.[40, 41] The nonbonded interaction cutoff was set to 1.2 nm, and the Particle Mesh Ewald algorithm[42] was used for electrostatic calculations with a grid space of 1 Å. We used the ColVar module[43, 44] to constrain the α-carbons of the tubulin cores by a harmonic bias, with a scaled normalized force constant of 0.05 kcal.mol^{-1} based on a collective variable on the overall orientation angle of the complex, in order to avoid a rotation of the system that would lead to self-interaction with the image systems from the periodic boundary conditions. This protocol was repeated for each of the three initial structures generated for the R2/tubulin complex (without CTTs, with the

Table 2: Summary of the MD simulations performed in the study. For each setup (column), we ran three replicas of 200 ns.

	tau-R2 in solution	tau-R2/tubulin complexes		
		Tubulins without CTTs	βI-αI-βI isotype	βIII-αI-βIII isotype
Box size	100x100x100Å^3	130x130x190Å^3	130x130x190Å^3	140x140x210Å^3
Protein atoms	446	20377	21031	21227
Ions	Na^+ : 89 Cl^- : 93	Na^+ : 308 Cl^- : 267	Na^+ : 336 Cl^- : 266	Na^+ : 426 Cl^- : 356
Water molecules	31127	93635	92318	125253

βI/αI/βI CTTs, and with the βIII/αI/βIII CTTs). Altogether we have 600 ns of production in the NPT ensemble for each complex.

In addition, we also performed a MD simulation of tau in water (in a cubic water box of 10 nm side length) following the same protocol and using the three initial tau-R2 structures taken from the complex with the βI/αI/βI isotype. Table 2 presents a summary of all the simulations discussed in this paper.

Analysis We used VMD Analysis[45] tools and ad-hoc Python scripts using the MDAnalysis[46, 47] and Mdtraj[48] libraries to analyze the MD trajectories. The tubulin interface burial was calculated using the Cocomaps server.[49]

3. Results and discussion

MD simulations on tau-R2 in solution

The DSSP graphs resulting from the simulation of tau-R2 in solution highlight the disordered nature of the protein, as they display only transient secondary structure elements, which vary from one trajectory to the other. (see Figure 2). The lack of stability for the tau-R2 structure is also visible in the RMSD plots shown in Figure SI-1.

MD simulations on the tau-R2/tubulin complex

Electrostatic properties of tau-R2 and the tubulin heterotrimer The surface electrostatic potentials for tau-R2 and both isotypes of the tubulin heterotrimer were calculated separately using the structures in the complex and are shown on Figure 3. While tau-R2's surface is mostly positively charged due to six lysine residues (see inserts in Figure 3), the tubuline's surface displays a broad electronegative patch all around the tau-R2 binding site (see the upper panels of Figures 3a and b). In addition, the CTTs are also negatively charged, as they contain many glutamate residues.

Conformational stability of the tau-R2/tubulin assembly The complex overall structure remains stable during all the trajectories, both without and with CTTs, as shown by the RMSD profiles in Figure 4. However, this stability is mostly due to the folded tubulin cores (see panels d-f in Figure 4), as both the CTTs and the tau-R2 fragment display much higher RMSDs during the trajectory (panels g-k in Figure 4), thus highlighting their flexible and disordered nature.

Figures 5a-c show the evolution of Fnat, the fraction of native contacts (i.e. residues from the initial tau-R2/tubulin interface with heavy atoms less than 5 Å away) as a function of time for the tau-R2/tubulin interface. Fnat remains in the [0.4-0.6] range for all trajectory except for one replica (model 84 from the βIII/αI/βIII isotype), a value lower than those observed for protein complexes involving fully folded partners,[50] thus characterizing the fuzzy nature of the tau/tubulin interface.[27] Despite the decrease of the Fnat value, the total number of contacts formed between tau-R2 and tubulin remains stable along time (as shown in Figures 5d-e), with a slightly larger average value in the case of the systems including the tubulin CTTs, as these provide opportunities for more

Table 3: Average interaction energies (in kcal.mol^{-1}) between tau-R2 and the tubulin interactions with tau-R2 during the simulations.

Tau/tubulin complex	Total interaction energy	Electrostatic term	Van der Waals term
Tubulins without CTTs	-1237.16	-1172,60	-64,56
βI-αI-βI isotype	-1477,44	-1404,66	-72,76
βIII-αI-βIII isotype	-1696,20	-1625,77	-70,42

Meanwhile, Figure 6a shows the average RMSF values for the tubulin-bound tau-R2 fragment. The profiles highlight a stable binding core centered on residue Ser289, which corresponds to the R2 strong interacting region identified by Brotzakis et al.[51] in their study integrating Cryo-EM data into MD simulations. Interestingly, the RMSF values can be larger in the case of the systems including tubulin CTTs (see Figures 6 and SI-2) in particular for the N- and C-ter ends of tau-R2, which can interact with the CTTs from the first (starting from the left of Figure 1) β-tubulin and the α-tubulin subunits. These interactions then lead to a lift of tau-R2 from the tubulin-core surface and an increased RMSF, either on the N-terminal side of tau-R2 (see the trajectories starting from models 17 and 38 in Figures SI-2b-c), or on its C-terminal side (trajectories starting from models 22 and 16 in Figures SI-2b-c)

Finally, the interaction energies between tau-R2 and the tubulin are shown in Figure 7. The values are mostly due to the electrostatic term of the potential (with a van der Waals contribution accounting for less than 5% of the total energy, see Table 3), and concur with earlier computational work on similar systems by Bhandare et al.[52] using a different force field, thus showing the robustness of MD simulations for the investigation of protein assemblies. On Figure 7 and Table 3, we can see how the tubulin CTTs help stabilizing the system by increasing the global interaction energy by

roughly 15%, in agreement with experimental data obtained by FRET[53] and fluorescence correlation spectroscopy.[54]

Detailed view of the contacts between tau-R2 and the tubulin heterotrimer Figure 8 shows a map of the contacts formed between tau-R2 and the tubulin heterotrimer during the simulations, the three-dimensional distribution of the contact points over the tubulin surface is shown in Figure 9. The contacts between tau-R2 and the tubulin core are highly conserved in the three systems, and for both tubulin isotypes, the residues from the CTTs of first β-subunit (on the bottom of Figure 9b-c) and α-subunit are also involved in the interaction with tau-R2. In the R2 strong interacting region, residues from the α-subunit forming long lasting contacts, such as Glu423, Ala426, Ala427 and Lys430 correspond to tau binding residues identified using NMR spectroscopy by Lefevre et al.[55] Furthermore, tubulin forms very stable contacts with tau-R2 around its three serine residues, Ser285, Ser289 and Ser293, which have been identified as phosphorylation sites in tauopathies.[23-25, 56] We also investigated hydrogen bonds formed by the serine residues within tau-R2 and with the tubulin heterotrimer (see Figure SI-3). Ser289 forms a very stable hydrogen bond with Glu434 from the tubulin α-subunit. This interaction is further reinforced when adding the CTTs, as the tubulin αCTT interacts with the positively charged C-ter of tau-R2 and in particular prevents residue Lys298 to interact with αTub-Glu434 (see Figure 8). Inversely, adding the tubulin CTTs destabilizes the transient hydrogen bond formed between tau-R2 Ser293 and Lys392 from the second β-subunit (reading Figure 8 from the top), since the C-ter of tau-R2 will now be lifted from the tubulin surface to interact with the tubulin αCTT (see the snapshot in Figure 6b). This phenomenon also leads to the RMSF increase shown in Figure SI-2.

In addition to the R2 strong interacting region, Figures 8 and 9 also highlight a secondary tau binding site on the tubulin surface, located near the interface between the first β-tubulin and the α-tubulin subunits, and which concurs with the weakly interacting region R2w centered around R2-Lys280 and R2-Lys281 defined by Brotzakis et al.[51] Tau-R2 residues 274-281 from this R2w region were also shown to play an important part in microtubule dynamics in an experimental study by Panda et al.[57]

Impact of tau-R2 on the CTTs mobility pattern Tubulin CTTs play an important part in the regulation of MT stability, in particular through their mobility and conformational dynamics.[10, 58] As they protrude from the MT surface, they are sometimes labeled as *E-hooks*,[59] due to their rich content in negatively charged glutamic acid residues, and are involved in the recruitment of several MAPs.[60-62] Since the tau binding site on the tubulin surface lies close to the CTTs, the interaction between tau and tubulin is likely to have an effect on the CTTs mobility. To investigate this issue, we ran additional MD simulations (following the protocol described in the Material & and Methods) section for the βI/αI/βI and βIII/αI/βIII isotypes of the tubulin heterotrimer, but this time without tau-R2. The CTT mobility patterns for both isotypes during the trajectories without and with tau-R2 are shown in Figure SI-4 via the distribution of the position of the CTTs center of mass (COM), using the same representation mode as in ref. 9. Interestingly, the CTT of the first β-subunit displays the same shift toward the surface of the α-subunit that was already observed in ref. 9. In addition the αI-CTT mostly interacts with the tubulin surface close to the tubulin longitudinal polymerization interface (between the α-subunit and the second β-subunit), in agreement with an earlier study of Chen et al.,[58] which used both experimental and simulation approaches. Comparing the mobility patterns without and with R2, we can see how the binding of

tau-R2 on the tubulin surface seems to prevent the interaction between the tails of the α-subunit and the second β-subunit, with the αI-CTT slightly shifting its COM distribution toward the surface of the α-subunit.

For both tubulin isotypes, we also monitored the number of contacts formed between each one of the three CTTs and the tubulin core, or between the CTTs and the tubulin core and tau-R2, during the trajectories without and with bound tau-R2 on the tubulin surface respectively. The resulting probability density plots are shown in Figure 10a-f, while the number of contacts for each CTT as a function of time is available in Figures SI-5 and SI-6. For the simulations without tau-R2, and for both the βI/αI/βI and βIII/αI/βIII isotypes, the CTT of the first β-subunit presents a bimodal distribution (see Figure 10a) with a predominant, low contact number state (termed as the *free state*) and a high contact number state (termed as the *bound state*). In the free state, the CTT/ tubulin core contacts are only formed via residues lying at the base of the CTT, while in the bound state all the CTT residues can form contacts with the tubulin core or with R2 (as shown in the snapshots in Figure 10g and h). Adding tau-R2 on the tubulin surface leads to a clear shift of the distribution in favor of the CTT bound state for both isotypes (Figure 10d). In the case of the α-CTT (from the central tubulin subunit) the impact of tau binding on the contact number distribution is more important for the βI/αI/βI isotype (blue lines in Figures 10b and e). For the contacts formed by second β-subunit CTT, the βIII/αI/βIII isotypes appears more sensitive to the introduction of tau-R2 in the system (red lines in Figures 10c and f). However, one should keep in mind that only the base of this CTT can form contacts with tau-R2 (see Figures 8 and 9c), as it is located right at the end of the tubulin heterotrimer.

On several occasions, we could observe for both βI and βIII CTTs a specific type of bound state, where the CTT will wrap itself the N-ter extremity of R2 (see Figure 10h), thus stabilizing this weak contacts zone, and resulting in the lowered RMSD of R2 for model 22 from the βI/αI/βI isotype in the 120-200 ns range (see Figure 4h) or for model 38 from the βIII/αI/βIII isotype in the 30-200 ns range (see Figure 4i). This "wraping mechanism" could in part explain why Tau's affinity for MTs decreases when CTTs are removed.[13]

4. Conclusions

Tau is a disordered protein that plays a key role for the stabilization of microtubules and fine-tunes their interaction with other MAPs. Here, we used a combination of modeling approaches to investigate the binding modes of the tau-R2 repeat on a tubulin heterotrimer on the atomic level. In particular, the reconstruction and explicit modeling of the tubulin C-terminal tails (which are not included in the experimental structures available for the tau/tubulin system) for two different β-tubulin isotypes enable us to see how the tau-R2/tubulin assembly forms a fuzzy complex, with conformational variability arising both from tau-R2 and the disordered CTTs. We also show how these CTTs contribute to stabilizing the assembly despite bringing additional mobility in the system. Our detailed investigation of the tau-R2/tubulin interface highlights the central part played by the three serine residues of tau-R2, and in particular Ser289, which lies in the center of the R2 strongly interacting region of tau. In the future, we plan to explicitly model the phosphorylation of these serine residues and its impact on stability of the tau-R2 interface, in order to better understand on the molecular scale how tau hyperphosphorylation can lead to various pathologies by disrupting its interaction with

microtubules. While numerous studies highlight the role played by tubulin CTTs or tau as regulators of motor proteins motility on microtubules, very few consider both elements (the CTTs and tau) simultaneously. Our results regarding the CTTs mobility and contacts without or with tau-R2 show a strong interplay between the two partners. The shift in favor of the CTTs bound state induced by tau that we observe in our simulations supports the hypothesis formulated by Lessard and Berger[63] that tau-mediated kinesin regulation might be linked to a competitive interaction between tau and the motor protein for the CTTs. Consequently, further work will also investigate how tau phosphorylation can impact the tubulin CTT's mobility, since it has been shown experimentally to modulate kinesin motility along microtubules,[20] a phenomenon where the CTTs are likely to play a part.

Acknowledgments: This work was supported by the ANR (MAGNETAU-ANR-21-CE29-0024) and by the "Initiative d'Excellence" program from the French State (Grant "DYNAMO", ANR-11-LABX-0011-01). Simulations were performed using the HPC resources from LBT/HPC.

Supporting Information Available: Additional data regarding the tubulin modelling (RMSD on bulk tau-R2, RMSF of the MT-bound tau-R2, H-bonds formed by the serines in tau-R2, CTT mobility patterns on the MT surface, number of contacts formed by the CTTs) is available as a pdf file.

References

[1] Aylett, C. H., Lowe, J., and Amos, L. A. (2011) New insights into the mechanisms of cytomotive actin and tubulin filaments, *Int. Rev Cell. Mol. Biol. 292*, 1-71.
[2] Bera, A., and Gupta, M. L., Jr. (2022) Microtubules in Microorganisms: How Tubulin Isotypes Contribute to Diverse Cytoskeletal Functions, *Front Cell Dev Biol 10*, 913809.
[3] Gasic, I. (2022) Regulation of Tubulin Gene Expression: From Isotype Identity to Functional Specialization, *Front Cell Dev Biol 10*, 898076.
[4] Roll-Mecak, A. (2019) How cells exploit tubulin diversity to build functional cellular microtubule mosaics, *Curr. Opin. Cell Biol. 56*, 102-108.
[5] Vemu, A., Atherton, J., Spector, J. O., Moores, C. A., and Roll-Mecak, A. (2017) Tubulin isoform composition tunes microtubule dynamics, *Molecular biology of the cell 28*, 3564-3572.
[6] Mizuhara, Y., and Takano, M. (2021) Biased Brownian Motion of KIF1A and the Role of Tubulin's C-Terminal Tail Studied by Molecular Dynamics Simulation, *International journal of molecular sciences 22*.
[7] Janke, C. (2014) The tubulin code: molecular components, readout mechanisms, and functions, *Journal of Cell Biology 206*, 461-472.
[8] Janke, C., and Magiera, M. M. (2020) The tubulin code and its role in controlling microtubule properties and functions, *Nat Rev Mol Cell Biol 21*, 307-326.
[9] Laurin, Y., Eyer, J., Robert, C. H., Prevost, C., and Sacquin-Mora, S. (2017) Mobility and Core-Protein Binding Patterns of Disordered C-Terminal Tails in beta-Tubulin Isotypes, *Biochemistry 56*, 1746-1756.
[10] Fees, C. P., and Moore, J. K. (2018) Regulation of microtubule dynamic instability by the carboxy-terminal tail of beta-tubulin, *Life Sci Alliance 1*.
[11] Heale, K. A., and Alisaraie, L. (2020) C-terminal Tail of beta-Tubulin and its Role in the Alterations of Dynein Binding Mode, *Cell Biochem Biophys 78*, 331-345.
[12] Chau, M. F., Radeke, M. J., de Ines, C., Barasoain, I., Kohlstaedt, L. A., and Feinstein, S. C. (1998) The microtubule-associated protein tau cross-links to two distinct sites on each alpha and beta tubulin monomer via separate domains, *Biochemistry 37*, 17692-17703.
[13] Hinrichs, M. H., Jalal, A., Brenner, B., Mandelkow, E., Kumar, S., and Scholz, T. (2012) Tau protein diffuses along the microtubule lattice, *The Journal of biological chemistry 287*, 38559-38568.
[14] Bigman, L. S., and Levy, Y. (2020) Tubulin tails and their modifications regulate protein diffusion on microtubules, *Proc. Natl. Acad. Sci. U. S. A. 117*, 8876-8883.
[15] Bigman, L. S., and Levy, Y. (2021) Modulating Microtubules: A Molecular Perspective on the Effects of Tail Modifications, *J. Mol. Biol. 433*, 166988.
[16] Butner, K. A., and Kirschner, M. W. (1991) Tau protein binds to microtubules through a flexible array of distributed weak sites, *J. Cell Biol. 115*, 717-730.
[17] Barbier, P., Zejneli, O., Martinho, M., Lasorsa, A., Belle, V., Smet-Nocca, C., Tsvetkov, P. O., Devred, F., and Landrieu, I. (2019) Role of Tau as a Microtubule-Associated Protein: Structural and Functional Aspects, *Front Aging Neurosci 11*, 204.
[18] Vershinin, M., Carter, B. C., Razafsky, D. S., King, S. J., and Gross, S. P. (2007) Multiple-motor based transport and its regulation by Tau, *Proc. Natl. Acad. Sci. U. S. A. 104*, 87-92.
[19] Dixit, R., Ross, J. L., Goldman, Y. E., and Holzbaur, E. L. (2008) Differential regulation of dynein and kinesin motor proteins by tau, *Science 319*, 1086-1089.
[20] Stern, J. L., Lessard, D. V., Hoeprich, G. J., Morfini, G. A., and Berger, C. L. (2017) Phosphoregulation of Tau modulates inhibition of kinesin-1 motility, *Molecular biology of the cell 28*, 1079-1087.
[21] Balabanian, L., Lessard, D. V., Swaminathan, K., Yaninska, P., Sebastien, M., Wang, S., Stevens, P. W., Wiseman, P. W., Berger, C. L., and Hendricks, A. G. (2022) Tau differentially regulates the transport of early endosomes and lysosomes, *Molecular biology of the cell 33*, ar128.
[22] Guo, T., Noble, W., and Hanger, D. P. (2017) Roles of tau protein in health and disease, *Acta Neuropathol 133*, 665-704.
[23] Hu, W., Zhang, X., Tung, Y. C., Xie, S., Liu, F., and Iqbal, K. (2016) Hyperphosphorylation determines both the spread and the morphology of tau pathology, *Alzheimers Dement 12*, 1066-1077.
[24] Drummond, E., Pires, G., MacMurray, C., Askenazi, M., Nayak, S., Bourdon, M., Safar, J., Ueberheide, B., and Wisniewski, T. (2020) Phosphorylated tau interactome in the human Alzheimer's disease brain, *Brain 143*, 2803-2817.
[25] Wesseling, H., Mair, W., Kumar, M., Schlaffner, C. N., Tang, S., Beerepoot, P., Fatou, B., Guise, A. J., Cheng, L., Takeda, S., Muntel, J., Rotunno, M. S., Dujardin, S., Davies, P., Kosik, K. S., Miller, B. L., Berretta, S., Hedreen, J. C., Grinberg, L. T., Seeley, W. W., Hyman, B. T., Steen, H., and Steen, J. A. (2020) Tau PTM Profiles Identify Patient Heterogeneity and Stages of Alzheimer's Disease, *Cell 183*, 1699-1713 e1613.
[26] Tompa, P., and Fuxreiter, M. (2008) Fuzzy complexes: polymorphism and structural disorder in protein-protein interactions, *Trends Biochem. Sci. 33*, 2-8.

[27] Sacquin-Mora, S., and Prevost, C. (2021) When Order Meets Disorder: Modeling and Function of the Protein Interface in Fuzzy Complexes, *Biomolecules 11*, 1529.
[28] Berman, H. M., Battistuz, T., Bhat, T. N., Bluhm, W. F., Bourne, P. E., Burkhardt, K., Feng, Z., Gilliland, G. L., Iype, L., Jain, S., Fagan, P., Marvin, J., Padilla, D., Ravichandran, V., Schneider, B., Thanki, N., Weissig, H., Westbrook, J. D., and Zardecki, C. (2002) The Protein Data Bank, *Acta Crystallogr., sect. D: Biol. Crystallogr. 58*, 899-907.
[29] Kellogg, E. H., Hejab, N. M. A., Poepsel, S., Downing, K. H., DiMaio, F., and Nogales, E. (2018) Near-atomic model of microtubule-tau interactions, *Science 360*, 1242-1246.
[30] Fiser, A., and Sali, A. (2003) Modeller: generation and refinement of homology-based protein structure models, *Methods in Enzymology 374*, 461-491.
[31] Webb, B., and Sali, A. (2016) Comparative Protein Structure Modeling Using MODELLER, *Curr Protoc Protein Sci 86*, 2 9 1-2 9 37.
[32] (2015) UniProt: a hub for protein information, *Nucleic Acids Research 43*, D204-212.
[33] Van der Spoel, D., Lindahl, E., Hess, B., Groenhof, G., Mark, A. E., and Berendsen, H. J. C. (2005) GROMACS: Fast, flexible, and free, *J. Comp. Chem. 26*, 1701-1718.
[34] Lee, J., Cheng, X., Swails, J. M., Yeom, M. S., Eastman, P. K., Lemkul, J. A., Wei, S., Buckner, J., Jeong, J. C., Qi, Y., Jo, S., Pande, V. S., Case, D. A., Brooks, C. L., 3rd, MacKerell, A. D., Jr., Klauda, J. B., and Im, W. (2016) CHARMM-GUI Input Generator for NAMD, GROMACS, AMBER, OpenMM, and CHARMM/OpenMM Simulations Using the CHARMM36 Additive Force Field, *J Chem Theory Comput 12*, 405-413.
[35] Onufriev, A. V., and Izadi, S. (2018) Water models for biomolecular simulations, *WIREs Computational Molecular Science 8*, e1347.
[36] Phillips, J. C., Hardy, D. J., Maia, J. D. C., Stone, J. E., Ribeiro, J. V., Bernardi, R. C., Buch, R., Fiorin, G., Henin, J., Jiang, W., McGreevy, R., Melo, M. C. R., Radak, B. K., Skeel, R. D., Singharoy, A., Wang, Y., Roux, B., Aksimentiev, A., Luthey-Schulten, Z., Kale, L. V., Schulten, K., Chipot, C., and Tajkhorshid, E. (2020) Scalable molecular dynamics on CPU and GPU architectures with NAMD, *J. Chem. Phys. 153*, 044130.
[37] Huang, J., Rauscher, S., Nawrocki, G., Ran, T., Feig, M., de Groot, B. L., Grubmuller, H., and MacKerell, A. D., Jr. (2017) CHARMM36m: an improved force field for folded and intrinsically disordered proteins, *Nat Methods 14*, 71-73.
[38] Nam, K., Gao, J., and York, D. M. (2005) An Efficient Linear-Scaling Ewald Method for Long-Range Electrostatic Interactions in Combined QM/MM Calculations, *Journal of Chemical Theory and Computation 1*, 2-13.
[39] Ryckaert, J.-P., Ciccotti, G., and Berendsen, H. J. C. (1977) Numerical integration of the cartesian equations of motion of a system with constraints: molecular dynamics of n-alkanes, *J. Comput. Phys. 23*, 327-341.
[40] Andersen, H. C. (1980) Molecular dynamics simulations at constant pressure and/or temperature, *The Journal of Chemical Physics 72*, 2384-2393.
[41] Martyna, G. J., Tobias, D. J., and Klein, M. L. (1994) Constant pressure molecular dynamics algorithms, *The Journal of Chemical Physics 101*, 4177-4189.
[42] Essmann, U., Perera, L., Berkowitz, M. L., Darden, T., Lee, H., and Pedersen, L. G. (1995) A SMOOTH PARTICLE MESH EWALD METHOD, *J. Chem. Phys. 103*, 8577-8593.
[43] Fiorin, G., Klein, M. L., and Hénin, J. (2013) Using collective variables to drive molecular dynamics simulations, *Mol. Phys. 111*, 3345-3362.
[44] Henin, J., Lopes, L. J. S., and Fiorin, G. (2022) Human Learning for Molecular Simulations: The Collective Variables Dashboard in VMD, *J Chem Theory Comput 18*, 1945-1956.
[45] Humphrey, W., Dalke, A., and Schulten, K. (1996) VMD: visual molecular dynamics, *J. Mol. Graph. 14*, 33-38, 27-38.
[46] Gowers, M. A Python Package for the Rapid Analysis of Molecular Dynamics Simulations, *Proc. 15th Python Sci. Confer*, 98.
[47] Michaud-Agrawal, N., Denning, E. J., Woolf, T. B., and Beckstein, O. (2011) MDAnalysis: A toolkit for the analysis of molecular dynamics simulations, *J. Comput. Chem. 32*, 2319-2327.
[48] McGibbon, R. T., Beauchamp, K. A., Harrigan, M. P., Klein, C., Swails, J. M., Hernandez, C. X., Schwantes, C. R., Wang, L. P., Lane, T. J., and Pande, V. S. (2015) MDTraj: A Modern Open Library for the Analysis of Molecular Dynamics Trajectories, *Biophys. J. 109*, 1528-1532.
[49] Vangone, A., Spinelli, R., Scarano, V., Cavallo, L., and Oliva, R. (2011) COCOMAPS: a web application to analyze and visualize contacts at the interface of biomolecular complexes, *Bioinformatics 27*, 2915-2916.
[50] Prevost, C., and Sacquin-Mora, S. (2021) Moving pictures: Reassessing docking experiments with a dynamic view of protein interfaces, *Proteins 89*, 1315-1323.
[51] Brotzakis, Z. F., Lindstedt, P. R., Taylor, R. J., Rinauro, D. J., Gallagher, N. C. T., Bernardes, G. J. L., and Vendruscolo, M. (2021) A Structural Ensemble of a Tau-Microtubule Complex Reveals Regulatory Tau Phosphorylation and Acetylation Mechanisms, *ACS Cent Sci 7*, 1986-1995.

[52] Bhandare, V. V., Kumbhar, B. V., and Kunwar, A. (2019) Differential binding affinity of tau repeat region R2 with neuronal-specific beta-tubulin isotypes, *Scientific reports 9*, 10795.
[53] Di Maio, I. L., Barbier, P., Allegro, D., Brault, C., and Peyrot, V. (2014) Quantitative analysis of tau-microtubule interaction using FRET, *International journal of molecular sciences 15*, 14697-14714.
[54] Fung, H. Y. J., McKibben, K. M., Ramirez, J., Gupta, K., and Rhoades, E. (2020) Structural Characterization of Tau in Fuzzy Tau:Tubulin Complexes, *Structure 28*, 378-384 e374.
[55] Lefevre, J., Chernov, K. G., Joshi, V., Delga, S., Toma, F., Pastre, D., Curmi, P. A., and Savarin, P. (2011) The C terminus of tubulin, a versatile partner for cationic molecules: binding of Tau, polyamines, and calcium, *The Journal of biological chemistry 286*, 3065-3078.
[56] Abreha, M. H., Ojelade, S., Dammer, E. B., McEachin, Z. T., Duong, D. M., Gearing, M., Bassell, G. J., Lah, J. J., Levey, A. I., Shulman, J. M., and Seyfried, N. T. (2021) TBK1 interacts with tau and enhances neurodegeneration in tauopathy, *The Journal of biological chemistry 296*, 100760.
[57] Panda, D., Goode, B. L., Feinstein, S. C., and Wilson, L. (1995) Kinetic stabilization of microtubule dynamics at steady state by tau and microtubule-binding domains of tau, *Biochemistry 34*, 11117-11127.
[58] Chen, J., Kholina, E., Szyk, A., Fedorov, V. A., Kovalenko, I., Gudimchuk, N., and Roll-Mecak, A. (2021) alpha-tubulin tail modifications regulate microtubule stability through selective effector recruitment, not changes in intrinsic polymer dynamics, *Dev Cell 56*, 2016-2028 e2014.
[59] Okada, Y., and Hirokawa, N. (2000) Mechanism of the single-headed processivity: diffusional anchoring between the K-loop of kinesin and the C terminus of tubulin, *Proc. Natl. Acad. Sci. U. S. A. 97*, 640-645.
[60] Lakamper, S., and Meyhofer, E. (2005) The E-hook of tubulin interacts with kinesin's head to increase processivity and speed, *Biophys. J. 89*, 3223-3234.
[61] Ramey, V. H., Wang, H. W., Nakajima, Y., Wong, A., Liu, J., Drubin, D., Barnes, G., and Nogales, E. (2011) The Dam1 ring binds to the E-hook of tubulin and diffuses along the microtubule, *Molecular biology of the cell 22*, 457-466.
[62] Tajielyato, N., Li, L., Peng, Y., Alper, J., and Alexov, E. (2018) E-hooks provide guidance and a soft landing for the microtubule binding domain of dynein, *Scientific reports 8*, 13266.
[63] Lessard, D., and Berger, C. (2021) The Microtubule Associated Protein Tau Regulates KIF1A Pausing Behavior and Motility, *bioRxiv*, 2021.2008.2011.455914.

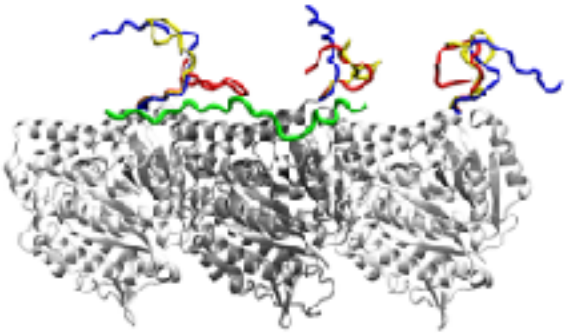

TOC image

Figure captions:

Figure 1: Starting structures for the tau-R2/tubulin assembly. The tubulin folded core is shown in dark and light grey for the α and β subunits respectively, while the disordered CTTs are shown in red, blue and yellow, and tau-R2 is shown in green. (a) βI/αI/βI isotype (b) βIII/αI/βIII isotype. Figures 1, 3, 9 and 10gh were prepared using Visual Molecular Dynamics.[45]

Figure 2: DSSP graphs from the three MD trajectories of tau-R2 in solution.

Figure 3: Surface electrostatic potential for the tubulin heterotrimer and tau-R2 (shown in the inserts), the complex orientation in the upper panels is the same as in Figure 1. Positive potentials are colored in blue and negative potentials in red. (a) βI/αI/βI isotype, (b) βIII/αI/βIII isotype.

Figure 4: Backbone RMSDs as a function of time for the tau-R2/tubulin complexes. Black and grey lines for the tubulin without CTTs, blue lines for the βI/αI/βI isotype and red lines for the βIII/αI/βIII isotype (this color code is also used for Figures 5-7 and 10). (a)-(c) Whole system, (d)-(f) tubulin core only, (g)-(i) tau-R2 only, (j)-(k) CTTs only.

Figure 5: Fraction of native contacts between tau-R2 and the tubulin heterotrimer as a function of time (a) Tubulin without CTTs (b) βI/αI/βI isotype (c) βIII/αI/βIII isotype. Total number of contacts between tau-R2 and the tubulin heterotrimer as a function of time (d) Tubulin without CTTs (e) βI/αI/βI isotype (f) βIII/αI/βIII isotype.

Figure 6: (a) RMSF of tau-R2, average value over the three simulations for each system. The three serine residues that are phosphorylated in tauopathies are highlighted in green along the sequence and shown as van der Waals spheres in the upper panel. (b) Snapshot from the trajectory starting with model 22 (for the βI/αI/βI isotype), where the R2-CTT (in black) is lifted from the tubulin surface.

Figure 7: Interaction energy between tau-R2 and the tubulin heterotrimer. Left panel: tubulin without CTTs, central panel: βI/αI/βI isotype, right panel: βIII/αI/βIII isotype.

Figure 8: Contact maps for the tau-R2/tubulin interface. The map only lists tubulin residues that are in contact with tau-R2 at least once during one of the nine MD trajectories. The tubulin CTTs for the βI/αI/βI and βIII/αI/βIII isotypes (central and right panels) are delimited by a purple frame, while the potentially phosphorylated serines (Ser 285, 289 and 293) of tau-R2 are highlighted by green frames. (a) Tubulin without CTTs (b) βI/αI/βI isotype (c) βIII/αI/βIII isotype.

Figure 9: 3-D distribution of the tubulin residues forming contacts with tau-R2 during the MD simulations. Transient contacts (less than 50% of the trajectory) are shown as green van der Waals spheres, while long lasting contacts are highlighted with a color scale ranging from orange (contacts formed during 50% of the trajectory) to red (permanent contacts). Serines 285, 289 and 293 of tau-R2 are shown as blue van der Waals spheres. (a) Tubulin without CTTs (b) βI/αI/βI isotype (c) βIII/αI/βIII isotype.

Figure 10: Probability density for the number of contacts formed by each CTT in the βI/αI/βI isotype (blue lines) and the βIII/αI/βIII isotype (red lines):

Simulations without tau-R2, contacts formed between the CTT and the tubulin core (a) First β-subunit, (b) α-subunit (c) second β-subunit.

Simulations with tau-R2, contacts formed between the CTT and the tubulin core or between the CTT and tau-R2 (d) First β-subunit, (e) α-subunit (f) second β-subunit.

Snapshots from the trajectory with the βI/αI/βI isotype and bound tau-R2 starting from model 22. The CTT from the first β-subunit is higlighted in red , (g) free CTT state, (h) bound CTT state

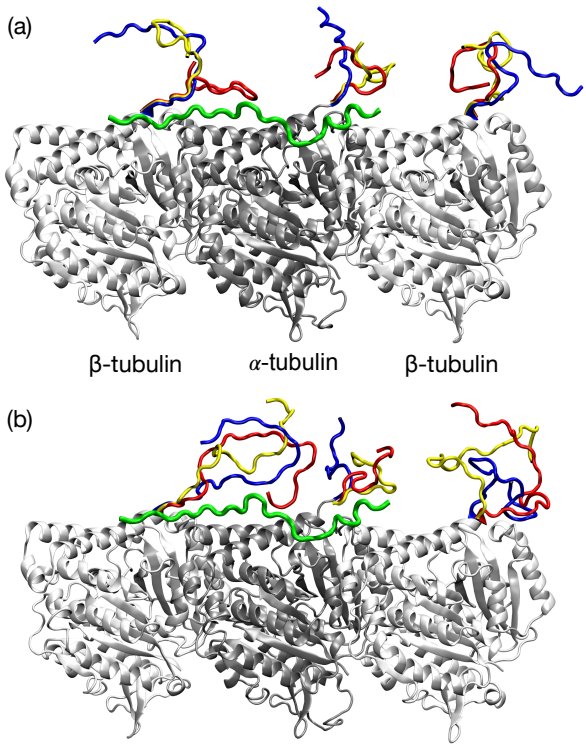

Figure 1

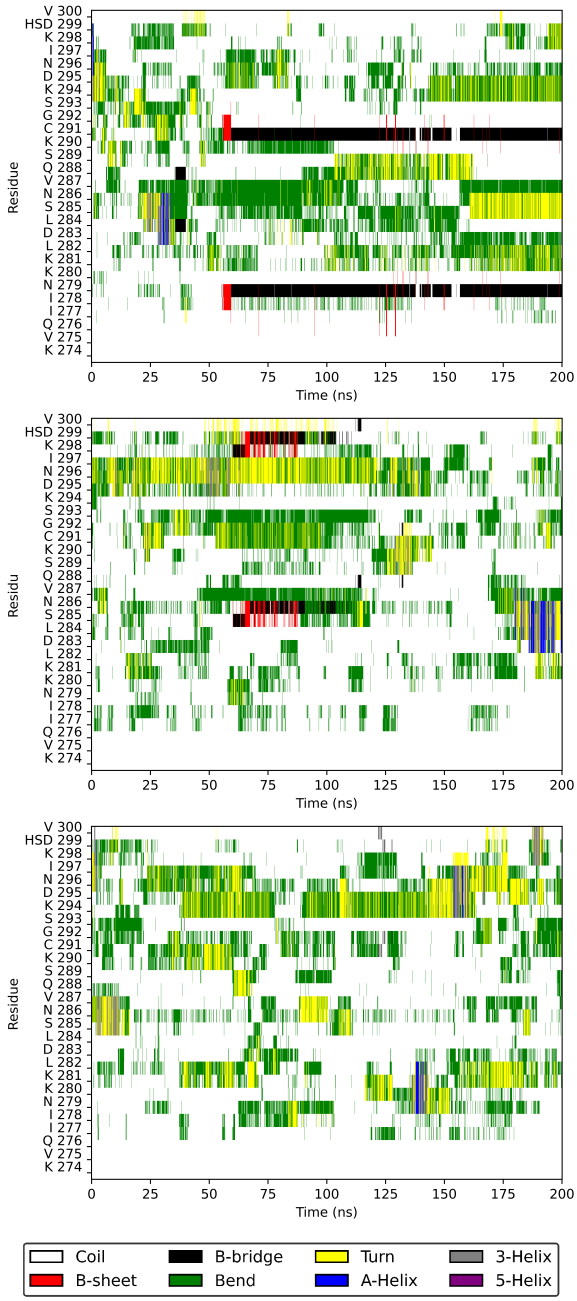
V 300
HSD 299
K 298
I 297
N 296
D 295
K 294
S 293
G 292
C 291
K 290
S 289
Q 288
V 287
N 286
S 285
L 284
D 283
L 282
K 281
K 280
N 279
I 278
I 277
Q 276
V 275
K 274
Residue
0
25
50
75
100
125
150
175
200
Time (ns)
Residu
Coil
B-bridge
Turn
3-Helix
B-sheet
Bend
A-Helix
5-Helix

Figure 2

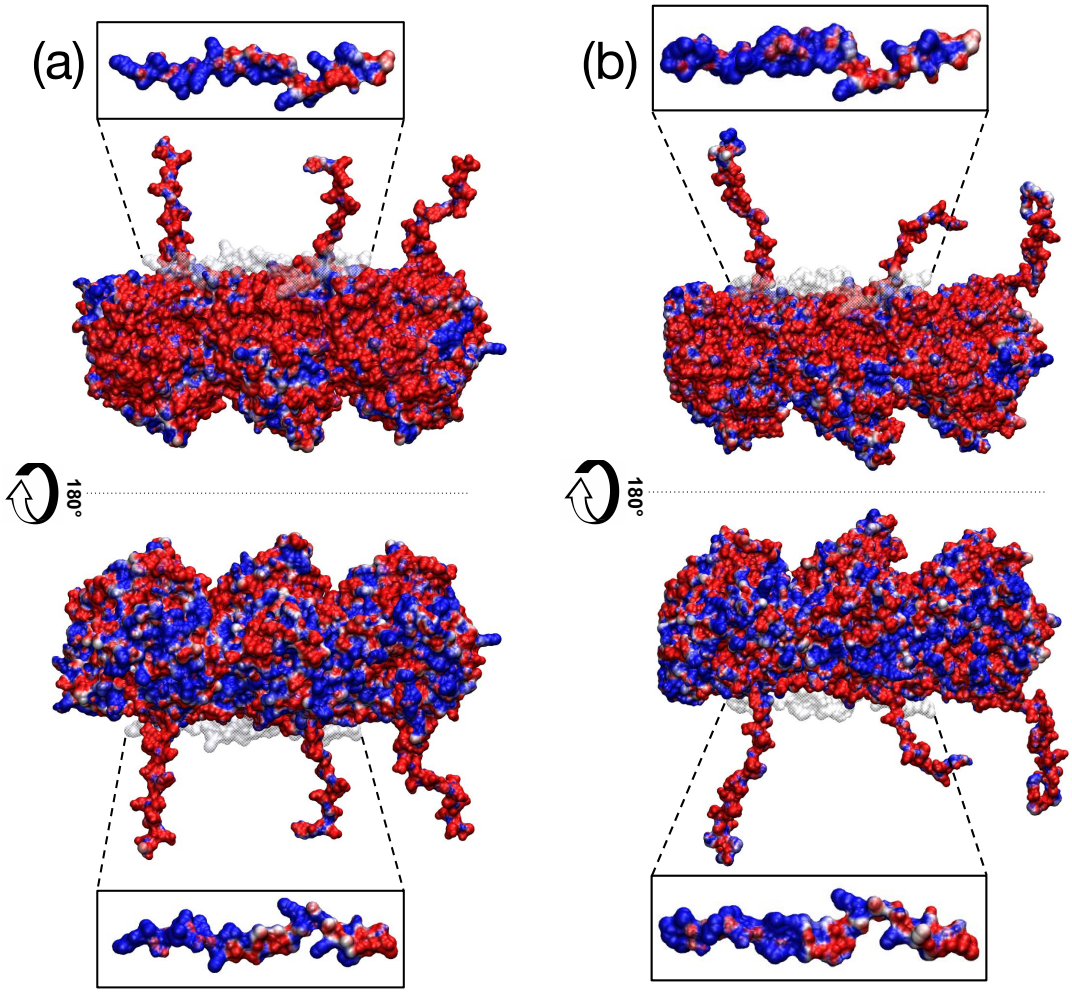

Figure 3

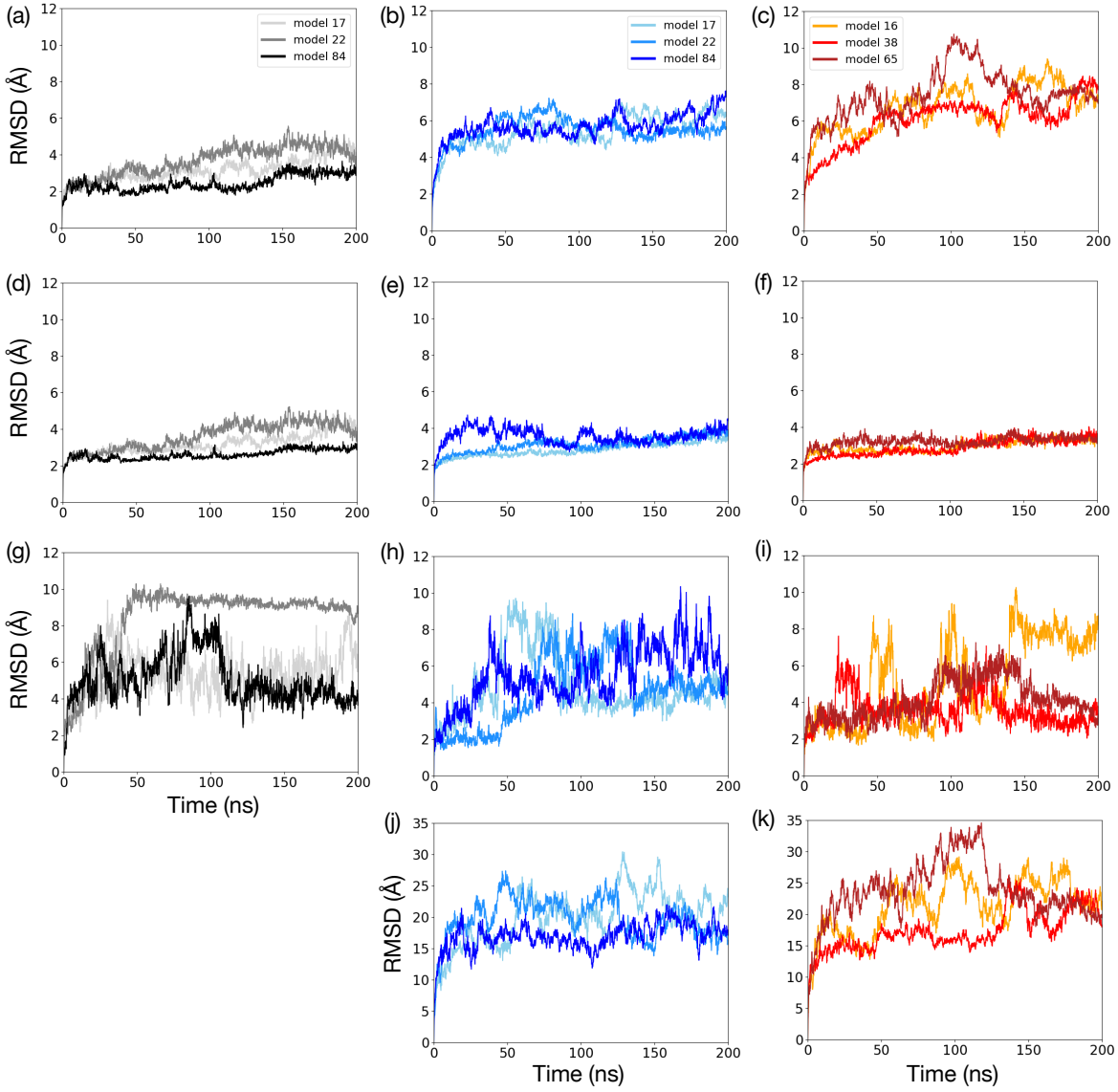
(a)
(b)
(c)
(d)
(e)
(f)
(g)
(h)
(i)
(j)
(k)
model 17
model 22
model 84
model 16
model 38
model 65
RMSD (Å)
Time (ns)

Figure 4

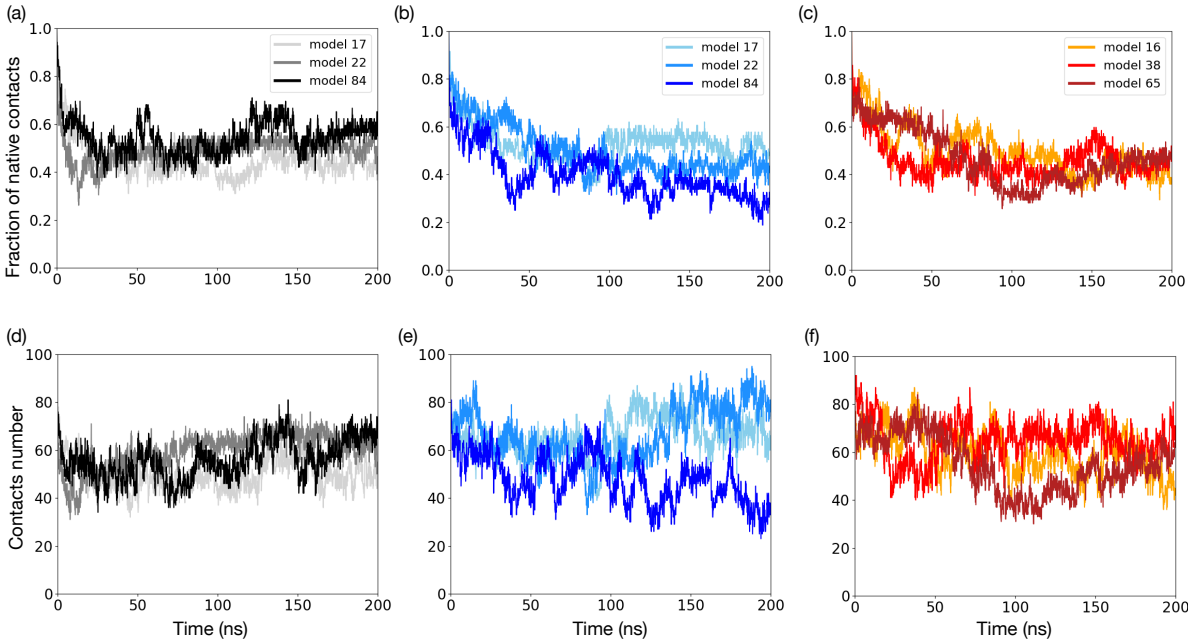
(a)
(b)
(c)
(d)
(e)
(f)
Fraction of native contacts
Contacts number
Time (ns)
model 17
model 22
model 84
model 16
model 38
model 65

Figure 5

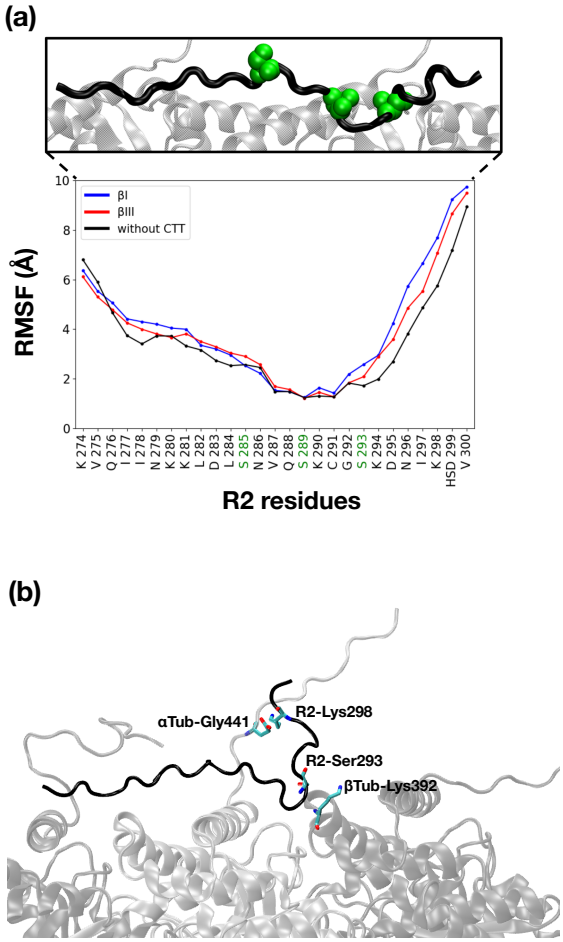
(a)
βI
βIII
without CTT
RMSF (Å)
R2 residues
(b)
αTub-Gly441
R2-Lys298
R2-Ser293
βTub-Lys392

Figure 6

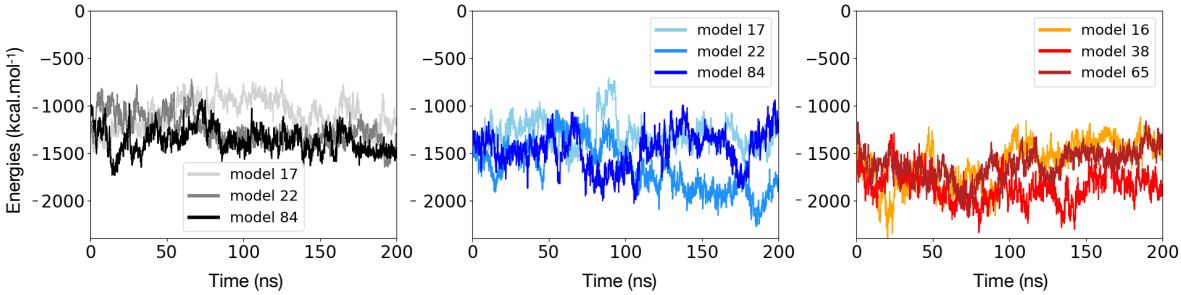
Energies (kcal.mol-1)
0
−500
-1000
-1500
-2000
0
50
100
150
200
Time (ns)
model 17
model 22
model 84
model 16
model 38
model 65

Figure 7

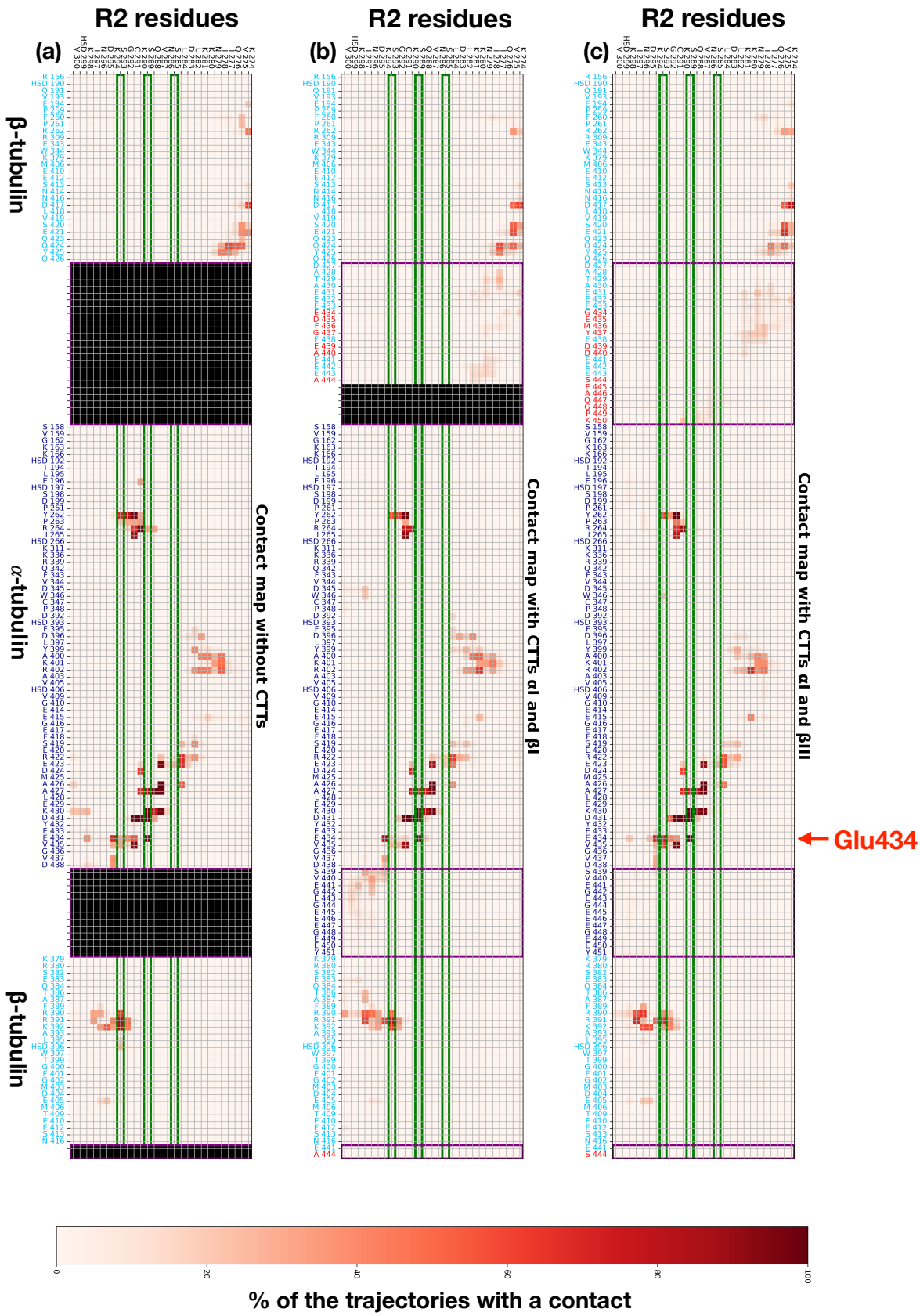
R2 residues
(a)
(b)
(c)
β-tubulin
α-tubulin
β-tubulin
Contact map without CTTs
Contact map with CTTs αI and βI
Contact map with CTTs αI and βIII
Glu434
0
20
40
60
80
100
% of the trajectories with a contact

Figure 8

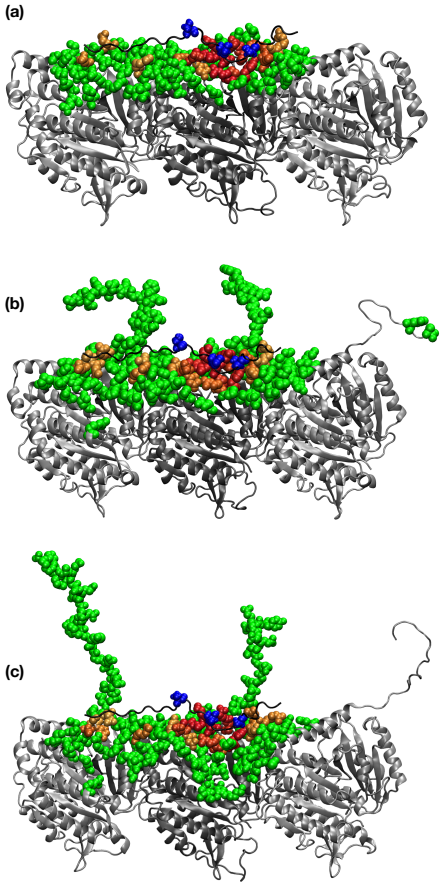

Figure 9

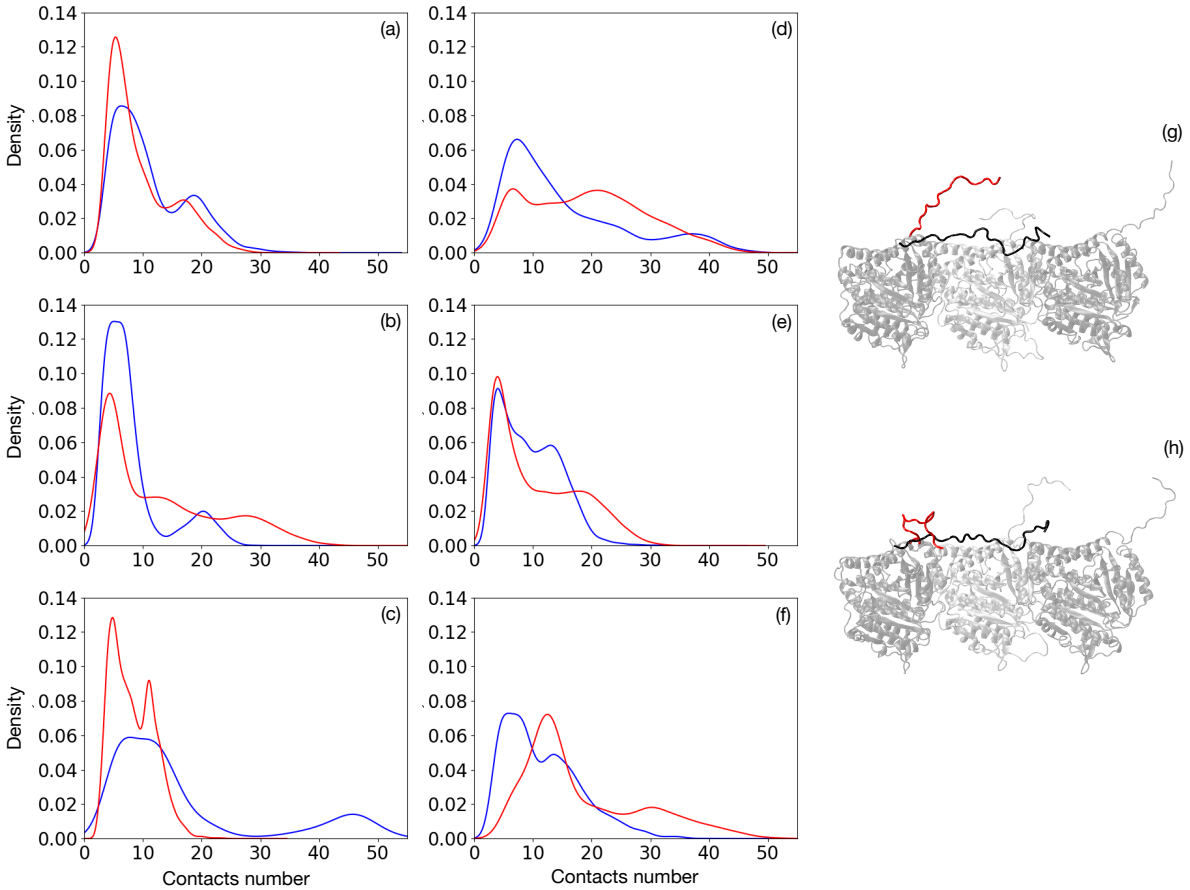
(a)
(b)
(c)
(d)
(e)
(f)
(g)
(h)
Density
Contacts number
0.00
0.02
0.04
0.06
0.08
0.10
0.12
0.14
0
10
20
30
40
50

Figure 10